European Cells and Materials Vol.50 2025 (pages 109–123) DOI: 10.22203/eCM.v050a07 ISSN 1473-2262

Original Article

NANO-ENCAPSULATED ACTIVE PROTEIN AMPK INHIBITS CARTILAGE MATRIX DEGRADATION IN EXPERIMENTAL OSTEOARTHRITIS RATS VIA SIRT1-REGULATED NEXILIN EXPRESSION NANO-AMPK INHIBITS CARTILAGE MATRIX DEGRADATION

X. You[1,§], L.Q. Wu[2,§], L.L. Fu[1], Q.Q. Wu[1] and B.R. Qi[1,*]

[1]Central Laboratory, Hainan Branch, Shanghai Children's Medical Center, School of Medicine, Shanghai Jiao Tong University, 572000 Sanya, Hainan, China

[2]Department of Orthopedics, Sanya Central Hospital (The Third People's Hospital of Hainan Province), 572000 Sanya, Hainan, China

[§]These authors contributed equally.

Abstract

Background: Osteoarthritis (OA) is characterized by progressive cartilage matrix degradation. Although adenosine monophosphate-activated protein kinase (AMPK) shows promise in treating OA, its clinical application is limited by poor bioavailability. Nano-encapsulation may overcome this limitation, but the underlying molecular mechanisms remain unclear. **Methods:** OA was induced in rats using the anterior cruciate ligament transection (ACLT) model, followed by intra-articular injection of nano-AMPK. Cartilage degradation was assessed by Masson staining and immunohistochemistry. The molecular mechanism was investigated using interleukin-1 beta (IL-1β)-induced rat chondrocytes, with or without sirtuin 1 (SIRT1) inhibitor (EX527) treatment and Nexilin silencing. The expression of cartilage matrix components, degradative enzymes, and signaling molecules was analyzed by Western blot and quantitative real-time polymerase chain reaction (qRT-PCR). **Results:** Nano-AMPK treatment significantly reduced cartilage degradation in ACLT rats, which was evidenced by increased collagen type II alpha 1 chain (COL2A1) and aggrecan expression and decreased matrix metalloproteinase (MMP)-3, MMP-13, and a disintegrin and metalloproteinase with thrombospondin motifs (ADAMTS) levels. *In vitro* studies revealed that nano-AMPK protected against IL-1β-induced matrix degradation by upregulating SIRT1 and Nexilin expression. Either SIRT1 inhibition or Nexilin silencing abolished the protective effects of nano-AMPK, indicating that the SIRT1-Nexilin pathway mediates nano-AMPK's chondroprotective effects. **Conclusions:** This study demonstrated that nano-encapsulated AMPK effectively prevented cartilage matrix degradation in experimental OA through a previously unidentified SIRT1-regulated Nexilin pathway, providing new insights into OA treatment strategies.

Keywords: Osteoarthritis, AMPK, anterior cruciate ligament transection, chondrocytes, sirtuin 1.

***Address for correspondence**: B.R. Qi, Central Laboratory, Hainan Branch, Shanghai Children's Medical Center, School of Medicine, Shanghai Jiao Tong University, 572000 Sanya, Hainan, China. Email: bangruoqi@126.com.

Introduction

Degenerative diseases like osteoarthritis (OA) are brought on by aging, genetics, and mechanical injury, among other things [1]. OA leads to disability in middle-aged and older adults, affecting their quality of life. Early diagnosis of OA is difficult, with symptoms including pain and cartilage degeneration [2]. Current treatments mainly focus on pain relief and do not halt disease progression. The only treatment for severe OA is joint replacement; however, this procedure is costly, and artificial joints can break down. Therefore, promoting cartilage repair and delaying OA progression are essential.

Adenosine monophosphate-activated protein kinase (AMPK) is an energy sensor crucial for regulating metabolism, maintaining energy balance, and responding to stress [3,4]. A study has indicated that AMPK is also involved in the skeletal system, controlling chondrocytes' energy metabolism and matrix metabolism, thereby affecting the health and function of cartilage [4]. The nicotinamide adenine dinucleotide (NAD+)-dependent deacety-

lase silent information regulator 1 (sirtuin 1 (SIRT1)) controls cell division, death, and metabolism [5]. There is a close interaction between SIRT1 and AMPK, and they jointly regulate cellular energy metabolism and stress responses [6,7]. Nexilin is an actin-associated protein primarily involved in the remodeling and stabilization of the cytoskeleton [8]. Although its exact involvement in chondrocytes is unknown, research has indicated that nexilin is essential for matrix metabolism and the chondrocyte stress response [9]. The rapid development of nanotechnology has provided new strategies for drug delivery and the encapsulation of biological macromolecules [10,11]. Recent advances in nanotechnology have revolutionized OA treatment approaches. Various nanocarrier systems, including polymeric nanoparticles, liposomes, and hydrogels, have been explored for targeted drug delivery to articular cartilage. However, most existing approaches focus on delivering small-molecule drugs or growth factors, and the potential of nano-encapsulated active proteins remains largely unexplored. Additionally, previous studies have investigated AMPK's role in OA [12,13], but the delivery challenges associated with protein therapeutics have limited its clinical application. Our nano-AMPK system addresses this critical gap by providing a novel protein delivery platform specifically designed for cartilage targeting.

Collagen type II alpha 1 chain (COL2A1) is the primary structural protein in articular cartilage, comprising approximately 90 % of the collagen network and playing a crucial role in maintaining cartilage integrity. In OA, the progressive loss of COL2A1 leads to compromised mechanical properties and reduced load-bearing capacity of the cartilage matrix. This degradation initiates a destructive cycle where mechanical stress further accelerates matrix breakdown, making COL2A1 maintenance a critical target for therapeutic intervention in OA.

In this study, the role of the AMPK-SIRT1-Nexilin pathway in OA and their relationship were systematically investigated by constructing an experimental OA rat model and using nanocoated active proteins to further reveal the possible mechanism of AMPK in OA. In addition to expanding our knowledge of the pathophysiological mechanisms underlying OA, this research will offer fresh perspectives and therapy possibilities.

Methods

Housing Conditions

Two groups of rats were used in this study: young Sprague-Dawley rats (2–3 weeks old, n = 6) for cell experiments and adult male Sprague-Dawley rats (200–250 g) for the anterior cruciate ligament transection (ACLT) model (n = 24). All rats were purchased from Shanghai MODEL ORGANISMS (Shanghai, China) and housed in the institutional animal facility under standard conditions: temperature 23 °C ± 1 °C, 12 h light/dark cycle, and 50 %–60 % relative humidity, with free access to standard rodent chow and water. Animals were acclimatized for 1 week before experiments. For the ACLT model, rats were randomly divided into four groups (n = 6 per group): sham, sham + nano-AMPK, model, and model + nano-AMPK. Post-surgery, rats were housed individually in ventilated cages with adequate food and water, and bedding was changed every 4 days.

Preparation of Nano-Encapsulated Active Protein AMPK

The preparation of nano-encapsulated active protein AMPK was conducted following previous research [11, 14]. Specifically, purified recombinant AMPK protein (ab184883, Abcam, Cambridge, MA, USA) and a nanoparticle encapsulation kit (FL-M16-001, Fluidiclab, Shanghai, China) were used. First, nanoparticles were prepared according to the instructions of the encapsulation kit, ensuring that all operations were performed under sterile conditions. In a sterile environment, an appropriate amount of AMPK protein was slowly added to the nanoparticle solution while gently mixing. The mixture was then incubated at room temperature or the specified temperature for a certain period to ensure the effective encapsulation of AMPK protein by the nanoparticles. The incubation time and temperature were adjusted according to the kit instructions.

Characterization of Nano-AMPK

The morphology of nano-AMPK was characterized using a field emission scanning electron microscope (SU8010, Hitachi, Tokyo, Japan) operated at an accelerating voltage of 5 kV with a working distance of 8–10 mm. Samples were prepared by placing a drop of the nanoparticle suspension onto a silicon wafer and allowing it to air-dry at room temperature. Prior to imaging, samples were sputter-coated with a thin layer of gold (approximately 5 nm thickness) using an ion sputter coater (E-1010, Hitachi, Tokyo, Japan) to enhance conductivity. Images were captured at various magnifications ranging from 5000× to 50,000×.

The direct fluid dynamics and size distribution of AMPK nanoparticles were studied by dynamic light scattering (DLS) using a Zetasizer Nano ZS90 (Malvern Instruments, Worcestershire, UK) dispersed in Milli-Q water at a scattering angle of 90°.

Encapsulation Efficiency (EE) Determination and Drug Loading (DL)

The DL and encapsulation rate of AMPK nanoparticles were determined by high-performance liquid chromatography. In 0.1 mL of methanol, 10 mg of freeze-dried nano-AMPK powder was dissolved. The samples were examined at a flow rate of 1.0 mL/min in a mobile phase that included 65 % (v/v) methanol and 35 % (v/v) ultra-pure water. The samples were tested on a detector (2996, Waters, Milford, MA, USA). Chromatographic separation was performed on a reversed-phase C18 column (4.6 × 250 mm–5

μm) at 25 °C. The calculation formula was as follows: EE = (total amount of drug − amount of free drug)/total amount of drug × 100 %. DL = (drug mass/total carrier mass) × 100 %.

Surgical Model of Anterior Cruciate Ligament Transection (ACLT)

Twenty-four 7-week-old male Sprague-Dawley rats (200–250 g) were divided into four groups (n = 6 per group): sham, sham + nano-AMPK, model, and model + nano-AMPK. Nano-AMPK treatment was administered via intra-articular injection into the knee joint cavity. Nano-AMPK was dissolved in sterile phosphate buffer saline (PBS) (pH 7.4) as the vehicle. The model + nano-AMPK and sham + nano-AMPK groups received intra-articular injections of nano-AMPK (200 mg/kg, 50 μL per injection) every 2 days for 12 weeks [15]. The control groups (sham and model groups) received intra-articular injections of the same volume (50 μL) of sterile PBS following the identical schedule. The stability of nano-AMPK in the PBS vehicle was confirmed by DLS analysis, showing unchanged hydrodynamic radius for at least 50 min at room temperature. The physical characteristics of the nano-AMPK preparation include average particle size (112.30 nm), zeta potential (50.74 mV), EE (55.48 % ± 0.27 %), and DL (42.54 % ± 0.29 %). In the sham and sham + nano-AMPK groups, only a skin incision was made without damaging the cruciate ligament. ACLT was performed on the right knee in the model and nano-AMPK groups. Post-surgery, rats were housed individually in a clean, temperature-controlled (23 °C ± 1 °C), and ventilated environment with adequate food and water, with bedding changed every 4 days. Prior to surgery, rats were anesthetized by intraperitoneal injection of sodium pentobarbital (40 mg/kg body weight). The depth of anesthesia was monitored by testing the pedal withdrawal reflex. Additional doses (10 mg/kg) were administered as needed to maintain adequate anesthesia throughout the surgical procedure. At the end of the experimental period, rats were humanely euthanized by intraperitoneal injection of an overdose of sodium pentobarbital (150 mg/kg body weight). Death was confirmed by the absence of heartbeat, breathing, and pedal withdrawal reflex for at least 5 min.

Histological and Immunohistochemical (IHC) Analyses

After 12 weeks, right hind limb samples were fixed with 4 % paraformaldehyde and stained with Masson staining and hematoxylin and eosin (H&E) staining to assess cartilage pathology. The Mankin score evaluated cartilage structure integrity, chondrocyte distribution, cartilage matrix staining, and tide line integrity; higher scores indicated more severe degeneration. Buffer was utilized as the negative control in the semi-quantitative marker assessment for IHC study. The primary antibodies were purchased from Abcam (Cambridge, MA, USA). The expression levels of expression and decreased matrix metalloproteinase (MMP)-3 (1:50 dilution, ab52915), aggrecan (1:500 dilution, ab186414), MMP-13 (1:100 dilution, ab315267), a disintegrin and metalloproteinase with thrombospondin motifs (ADAMTS)-4 (1:200 dilution, ab84792), and collagen type II alpha 1 chain (COL2A1, 1:200 dilution, ab307674) were observed under a microscope. The automatic cell counting function in Image-Pro Plus 6.0 software (Media Cybernetics, Rockville, MD, USA) was used to analyze the data.

Isolation and Culture of Chondrocytes

Primary chondrocytes were extracted from the femoral head and tibial plateau cartilage of Sprague-Dawley rats aged 14–21 days and kept free of pathogens. After cutting the cartilage, they were digested for 30 min at 37 °C using 0.25 % trypsin and 4 h using 0.2 % COL2A1 in Dulbecco's modified Eagle medium (DMEM)-F12. After being centrifuged for 5 min at 1200 rpm, the chondrocyte suspension was resuspended in DMEM-F12 containing 10 % fetal bovine serum (FBS) and 1 % penicillin-streptomycin, and it was then transferred into culture flasks. Cells were cultured at 37 °C in a 5 % CO_2 incubator. Chondrocytes were used for *in vitro* experiments no later than the second passage to minimize phenotypic loss. The cells were mycoplasma-free, and short tandem repeat (STR) analysis revealed that they were derived from its parental cells.

Establishment of Cell Model of OA

Chondrocytes were treated with 10 ng/mL interleukin-1 beta (IL-1β) to establish a model of OA [16]. Recombinant rat IL-1β was purchased from PeproTech (Cat. No. 400-01B, Rocky Hill, NJ, USA). IL-1β was reconstituted in sterile PBS containing 0.1 % bovine serum albumin to prepare stock solutions and stored at −80 °C until use. The model group consisted of chondrocytes treated with 10 ng/mL IL-1β for 24 h, whereas the control group consisted of chondrocytes in DMEM-F12 with 10 % FBS. The IL-1β + nano-AMPK group received 10 ng/mL IL-1β and 10 μg/mL nano-AMPK [17]. Nano-AMPK was dissolved in dimethyl sulfoxide (DMSO) and diluted in culture medium (10 % FBS and 1 % antibiotics). The IL-1β + nano-AMPK + EX527 group received 10 μM/mL EX527 [18] (2780/1, Tocris Bioscience, Ellisville, MO, USA) and 10 ng/mL IL-1β.

Cell Transfection

Chondrocytes were cultured to 75 % confluent before transfection with small interfering RNA (siRNA). Scramble siRNA served as the negative control group. SIRT1 siRNA: 5′-TGAAGTGCCTCAGATATTA-3′ and 5′-TAATATCTGAGGCACTTCA-3′. Lipofectamine 2000 (Thermo Fisher Scientific, Waltham, MA, USA) was transfected for 48 h.

CCK-8 Assay

Cell proliferation was measured by using a Cell Counting Kit-8 (CCK-8) (C0037, Biotechnology, Shanghai, China). The cell density of 96-well plates was 5×10^3 cells/well. We added 100 μL of fresh medium and 10 μL of CCK-8 solution, and the plates were incubated at 37 °C for 30 min. Absorbance was measured at 450 nm using a microplate reader (1681130, Bio-Rad, Hercules, CA, USA).

SIRT1 Activity Assay

SIRT1 activity was measured using a Fluorometric SIRT1 activity assay kit (Cat. No. CS1040; Sigma–Aldrich, St. Louis, MO, USA) following the manufacturer's instructions. Chondrocytes and histamine extracts were treated with Triton X-100 at a final concentration of 0.5 %. The samples were incubated at 23 °C with a reaction mixture containing acetylated peptide substrates for 30 min. The fluorescence intensity of SIRT1 (λex = 340 nm and λem = 450 nm) was measured using a microplate reader.

Western Blot Analysis

Using a protease inhibitor cocktail (HY-K0011, MedChemExpress, Monmouth Junction, NJ, USA) and RIPA lysis buffer (R0010, Solarbio, Beijing, China), the total proteins of cartilage tissue and chondrocytes were extracted. Supernatants were mixed with loading buffer and boiled. Proteins were separated by electrophoresis on 10 % sodium dodecyl sulfate polyacrylamide gel electrophoresis (SDS-PAGE) gel, transferred to a polyvinylidene fluoride (PVDF) membrane, and blocked with nonfat dry milk solution. Membranes were incubated overnight at 4 °C with primary antibodies: transforming growth factor beta ((TGF-β)1, NBP1-80289), Smad2 (NB100-56462), inducible nitric oxide synthase (iNOS, NB300-605), cyclooxygenase-2 (COX-2, NB100-689), MMP-3 (NB100-91878), and MMP-13 (NBP2-66954) (1:1000, Novus, Littleton, CO, USA); ADAMTS-4 (1:500, ab314856, Abcam, Cambridge, MA, USA); and COL2A1 (ab307674), SIRT1 (ab110304), and glyceraldehyde 3-phosphate dehydrogenase (GAPDH, #2118) (1:1000, CST, Danvers, MA, USA). After washing, HRP-labeled secondary antibodies goat anti-mouse IgG (1:2000, ZSGB-BIO, Beijing, China, Cat. No. ZB-2305) and goat anti-rabbit IgG (1:2000, ZSGB-BIO, Cat. No. ZB-2301) were applied, and membranes were visualized. Bands were assessed using a chemiluminescence kit (P0018, Beyotime, Shanghai, China) and analyzed with Image J software (version 1.5f, NIH, Bethesda, MD, USA).

Quantitative Real-Time Polymerase Chain Reaction (qRT-PCR)

Total RNA of chondrocytes was extracted using a Tiangen kit (DP419, Beijing, China). PrimeScript complementary deoxyribonucleic acid (cDNA) real time (RT) Master Mix (RR036, Kogen, Tokyo, Japan) was used to generate cDNA. SYBR PreMix Ex Taq^{TM} (RR390, Kogen, Tokyo, Japan), RNase-free water (RT121, Tiangen, Beijing, China), and certain primers were used for the amplification process. The PCR process was monitored with a LightCycler®480 (05015243001, Roche, Basel, Switzerland), and relative expression levels were calculated using the $2^{-\Delta\Delta Ct}$ method. Primer sequences are listed in Table 1.

Immunofluorescence (IF) Staining

The chondrocytes in each plate were fixed for 25 min with 4 % paraformaldehyde (P1110, Solarbio, Beijing, China), permeabilized for 30 min with 0.2 % Triton X-100 (T8200, Solarbio), and blocked for 1.5 h at room temperature. Primary antibodies (COL2A1, 1:100 dilution, ab307674, Abcam, Cambridge, MA, USA) were incubated at 4 °C for 24 h. Alexa Fluor 488-conjugated secondary antibody was diluted 1:500 in PBS. The secondary antibody was incubated in the dark for 1.5 h. After secondary antibody incubation, cells were washed three times with PBS (5 min each). Nuclei were counterstained with 4′,6-diamidino-2′-phenylindole (DAPI) (1 μg/mL in PBS) for 10 min at room temperature in the dark. After three final PBS washes (5 min each), coverslips were mounted using anti-fade mounting medium. Positively stained cells were detected and analyzed using an inverted fluorescence microscope (Eclipse Ts2, Nikon, Tokyo, Japan).

ELISA

For enzyme-linked immunosorbent assay (ELISA) analysis, cartilage tissue samples were collected from the knee joints after 12 weeks of treatment. The tissue samples were homogenized in ice-cold PBS and centrifuged at 5000 g for 10 min at 4 °C. The supernatants were collected for measurement of tumor necrosis factor alpha (TNF-α) (Cat. No. RTA00, R&D Systems, Minneapolis, MN, USA), iNOS (Cat. No. ab210882, Abcam, Cambridge, MA, USA), and COX-2 (Cat. No. KA0238, Abnova, Taipei, China) levels by using commercial ELISA kits according to the manufacturers' instructions.

Statistical Analysis

In vitro experiments were repeated at least three times and performed in technical replicates. Results are mean ± standard deviation (SD). Variance was checked with Bartlett's test ($p > 0.05$), followed by one-way analysis of variance (ANOVA) and Dunnett's test. A p-value < 0.05 was considered significant.

Results

Nano-AMPK Reduces Inflammation and ECM Degradation in Chondrocytes of OA Rats

First, we characterized the nano-AMPK nanoparticles. In this study, transmission electron microscopy (TEM) revealed that these nanoparticles were generally spherical,

Table 1. Primer sequences.

Gene	Forward (5′–3′)	Reverse (5′–3′)
SIRT1	TGGGACTCTGCACAACCTTTCTCA	AGTGTCGTGATGGCGTAGAACAGT
Nexilin	TCTGACAAAGCCTTCATGTCC-3′	TCTGATAGCTCGTCACAAGC
GAPDH	ATGACATCAAGAAGGTGGTG	CATACCAGGAAATGAGCTTG

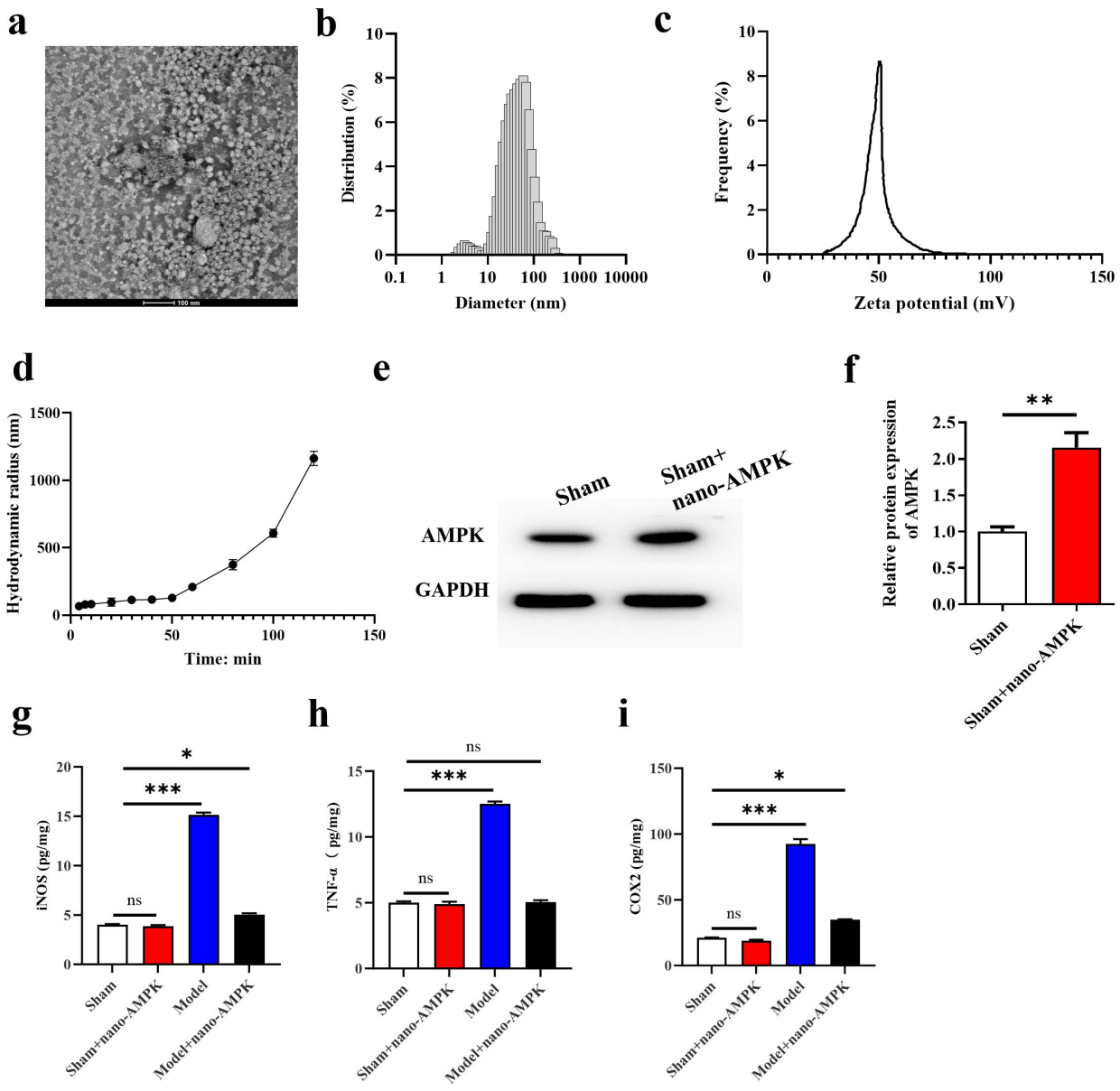

Fig. 1. Nano-AMPK mitigates inflammation and ECM degradation in chondrocytes of osteoarthritis rats. (**a**) Morphology under TEM. Scale bar: 100 nm. (**b**) Hydrodynamic size of the nano-AMPK detected by DLS. (**c**) Zeta potential value of nano-AMPK. (**d**) Hydrodynamic radius of nano-AMPK over time (120 min). (**e,f**) Western blot analysis of AMPK. (**g–i**) Expression levels of inducible nitric oxide synthase (iNOS), tumor necrosis factor alpha (TNF-α), and cyclooxygenase-2 (COX-2). AMPK, adenosine monophosphate-activated protein kinase; ECM, extracellular matrix; TEM, transmission electron microscopy; GAPDH, glyceraldehyde 3-phosphate dehydrogenase; SD, standard deviation; DLS, dynamic light scattering. Data are mean ± SD, ns = not significant, n = 6, *$p < 0.05$, **$p < 0.01$, and ***$p < 0.001$.

with diameters ranging from 50 nm to 100 nm (Fig. 1**a**). Fig. 1**b** shows that the average particle size of nano-AMPK was 112.30 nm. Fig. 1**c** shows that the charge distribution of nano-AMPK was 50.74 mV. In Fig. 1**d**, the hy-

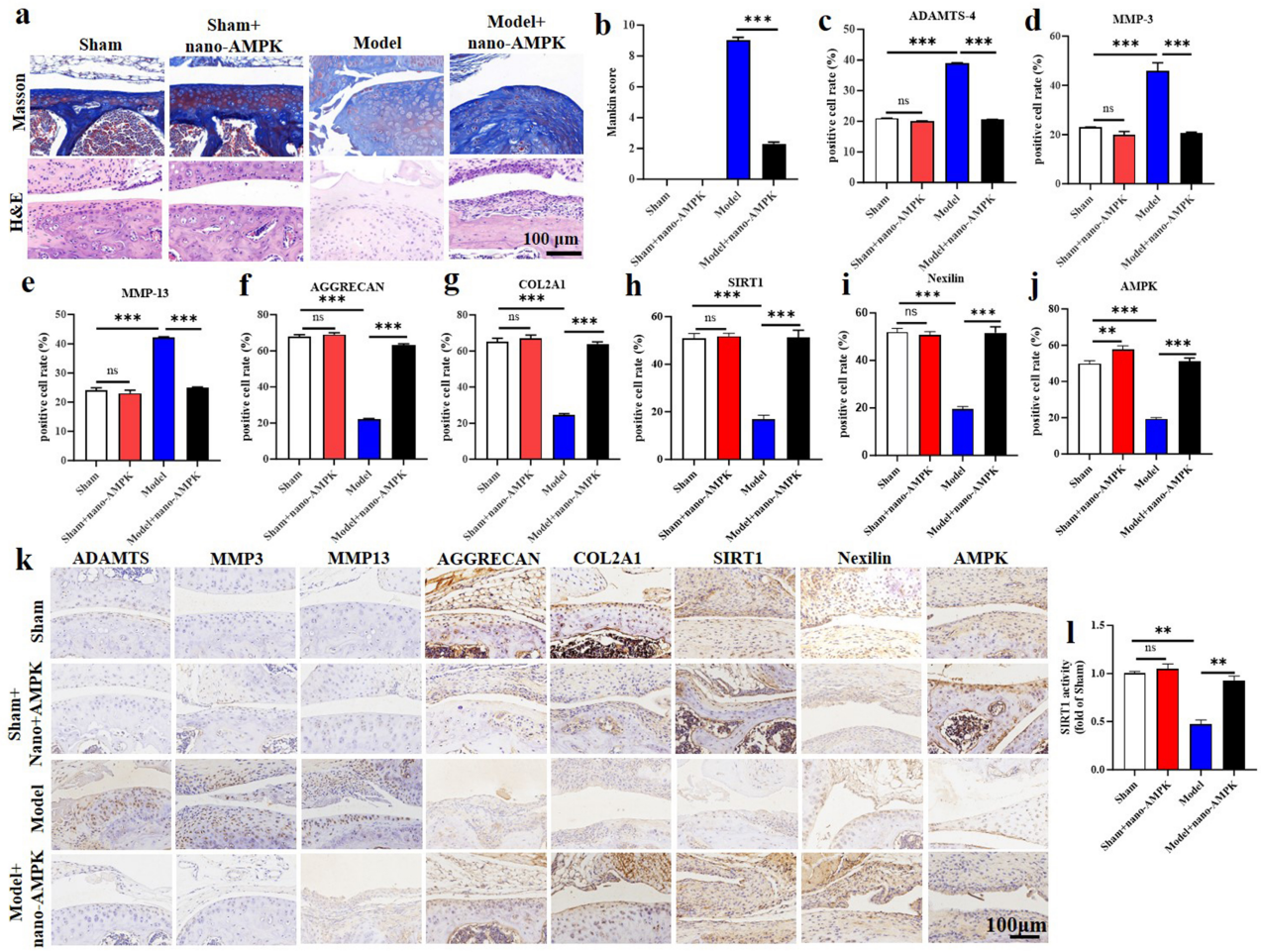

Fig. 2. Nano-AMPK reduced chondrocyte matrix degradation in the ACLT rat model. (**a**) Cartilage surfaces were examined by Masson staining. Scale bar: 100 μm. (**b**) Mankin score. (**c–k**) IHC staining and quantification of chondrocyte matrix degradation markers. Scale bar: 100 μm. (**l**) SIRT1 activity assay. ACLT, anterior cruciate ligament transection; H&E, hematoxylin and eosin; ADAMTS, a disintegrin and metalloproteinase with thrombospondin motifs; MMP, matrix metalloproteinase; COL2A1, collagen type II alpha 1 chain; SIRT1, sirtuin 1; IHC, immunohistochemical. Data are mean ± SD, n = 6, ns = not significant, $^{**}p < 0.01$, $^{***}p < 0.001$.

Table 2. Physicochemical property parameters of nanoparticles.

Parameters	Nano-AMPK
EE (%)	55.48 ± 0.27
DL (%)	42.54 ± 0.29

AMPK, adenosine monophosphate-activated protein kinase; EE, encapsulation efficiency; DL, drug loading.

drodynamic radius of nano-AMPK remained basically unchanged within 50 min, indicating that the structural integrity of nano-AMPK was stable within 50 min. In Table 2, the EE of nano-AMPK was 55.4 8% ± 0.27 % and the DL was 42.54 % ± 0.29 %. Western blot analysis verified the expression of AMPK (Fig. 1**e,f**). These results indicated that we successfully constructed the nano-AMPK nanoparticles. To investigate the effects of nano-AMPK on inflammation and extracellular matrix (ECM) degradation in OA rat chondrocytes, we performed ELISA assays. Comparing the model group with the sham group, Fig. 1**g–i** revealed that the model group had much greater levels of TNF-α, iNOS, and COX-2, whereas the nano-AMPK group had significantly lower levels.

Nano-AMPK Reduced Chondrocyte Matrix Degradation in the ACLT Rat Model

Masson and H&E staining (Fig. 2**a,b**) showed a smooth, undamaged cartilage surface with clear edges in the sham group. In the model group, chondrocytes were clustered, and red staining was markedly reduced. The model group had more hypertrophic cells and distorted tide lines, whereas the nano-AMPK group had fewer hypertrophic cells, with clustered chondrocytes and uniformly red-stained matrix. The Mankin score indicated higher scores in the model group than in the sham + nano-AMPK

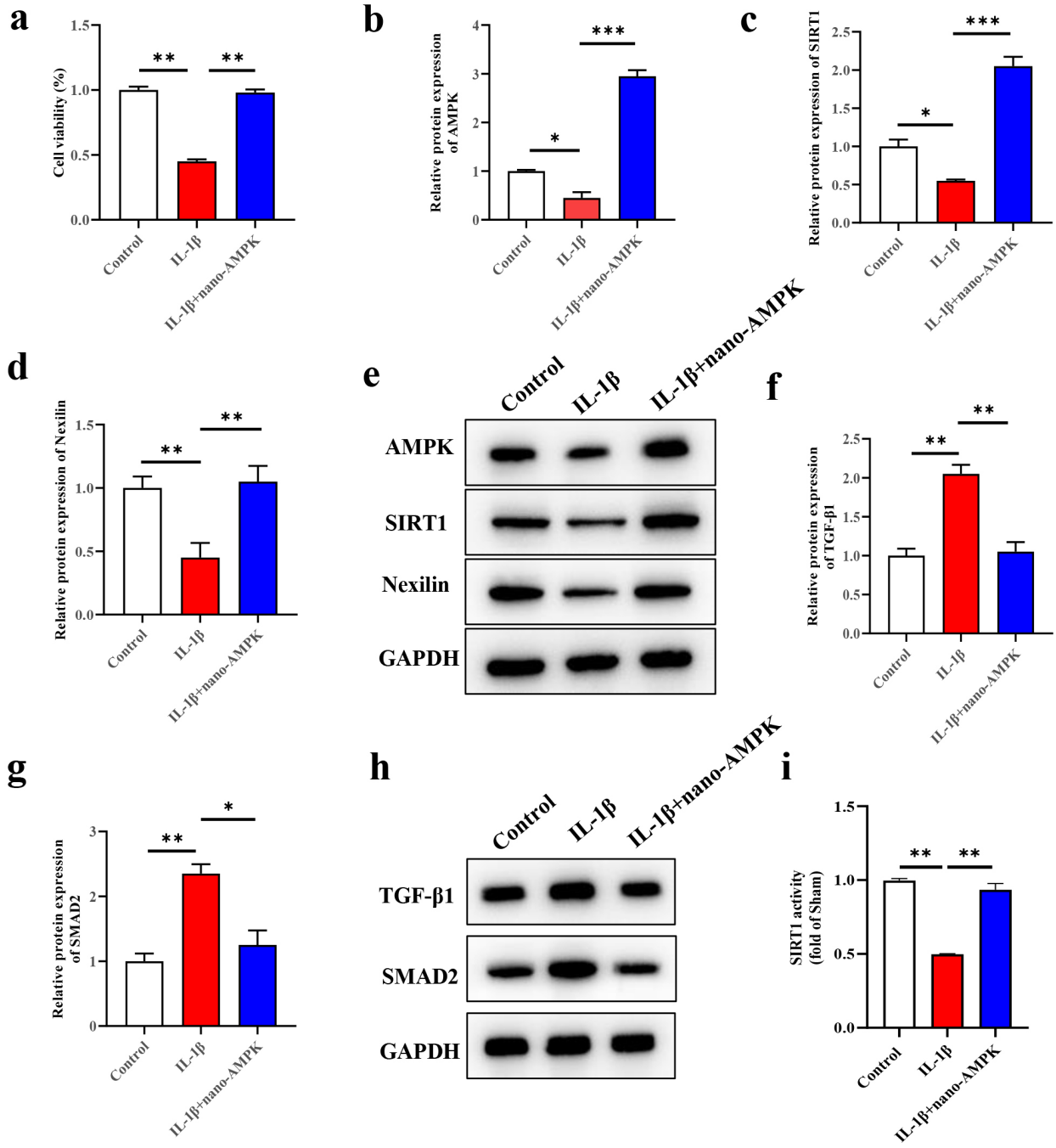

Fig. 3. Nano-AMPK boosted chondrocyte viability and increased SIRT1 expression. (**a**) The activity of chondrocytes after different treatments. (**b–e**) AMPK and SIRT1 protein levels in chondrocytes measured by qRT-PCR. (**f–h**) TGF-β and Smad2 protein levels in chondrocytes detected by Western blot and quantified using Image J. (**i**) SIRT1 activity assay in chondrocytes. IL-1β, interleukin-1 beta; TGF-β, transforming growth factor beta; qRT-PCR, quantitative real-time polymerase chain reaction. Data are mean ± SD (n = 3), *$p < 0.05$, **$p < 0.01$, and ***$p < 0.001$.

group ($p < 0.001$). IHC staining (Fig. 2**c–k**) revealed stronger COL2A1 and aggrecan expression in the sham and nano-AMPK groups, with more intense brown staining than the model group. Conversely, MMP-3, MMP-13, and ADAMTS were weakly positive in the sham and nano-AMPK groups, with less brown staining than the model group ($p < 0.001$). Notably, the positive cell rates of SIRT1, Nexilin, and AMPK were significantly reduced in the model group ($p < 0.001$), and their positive cell rates increased significantly after treatment with nano-AMPK ($p < 0.001$). The Mankin score matched the histological analysis results. Fig. 2**l** shows the effect of AMPK on SIRT1

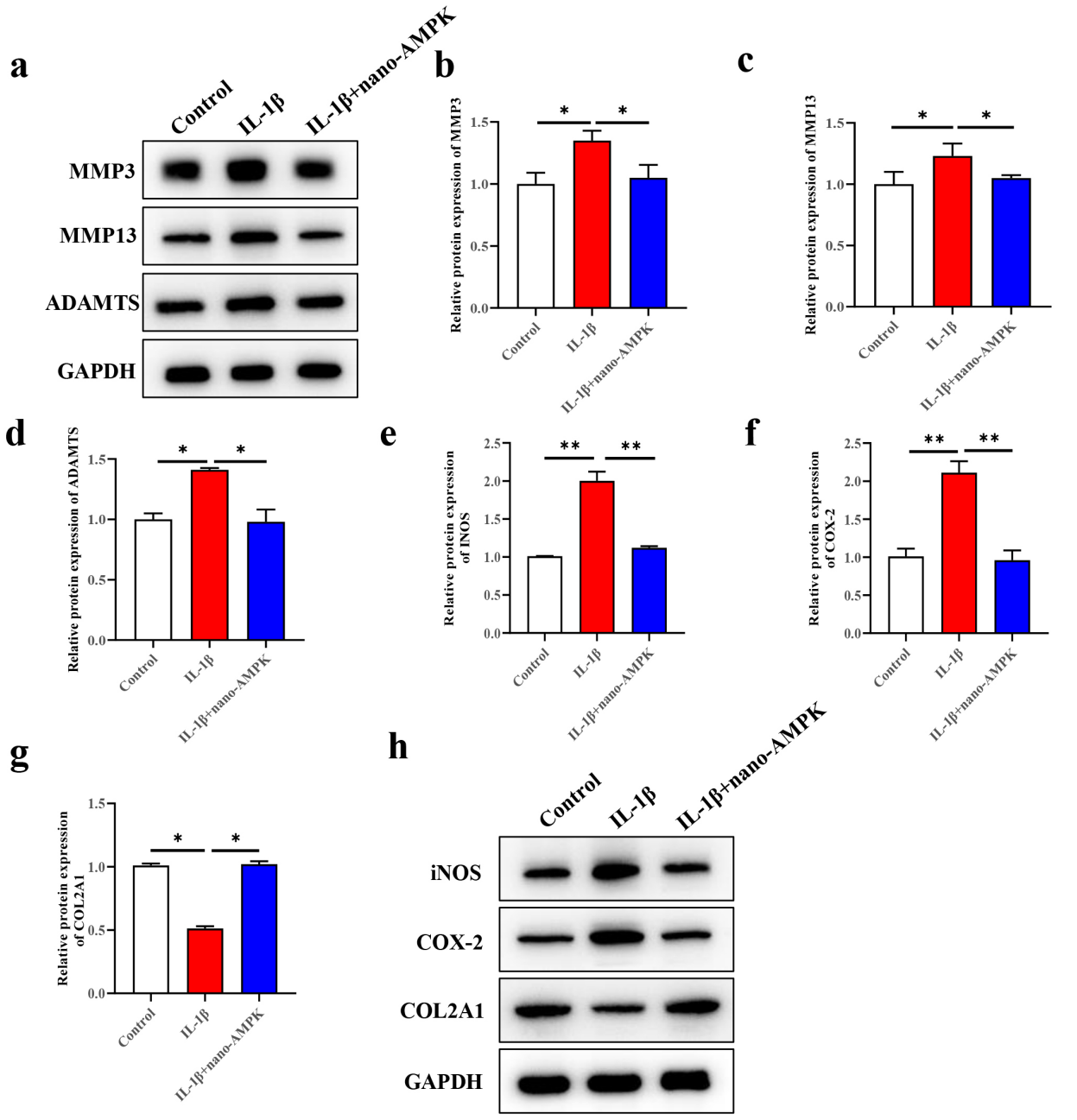

Fig. 4. Nano-AMPK suppresses matrix degradation markers. (**a–h**) Protein analysis of chondrocyte matrix degradation markers' expression levels in chondrocytes. N = 3, *$p < 0.05$, **$p < 0.01$.

activity. The activity of SIRT1 significantly decreased in the model group, whereas that was significantly enhanced after treatment with nano-AMPK ($p < 0.01$). To verify that the therapeutic effects were specifically attributed to AMPK rather than the delivery system, we conducted additional control experiments with nanocarrier administration alone. As shown in **Supplementary Fig. S1**, treatment with the nanocarrier without AMPK demonstrated no protective effects on articular cartilage in experimental OA rats, confirming that the observed therapeutic benefits in our main study were specifically due to the nano-AMPK intervention. To assess the potential systemic effects of our treatments, we performed histological analysis of vital organs. H&E staining of heart and lung tissues from all treatment groups showed no pathological alterations (**Supplementary Fig. S2**). The tissue architecture remained intact and comparable to control groups, with no signs of inflammation, cellular damage, or structural abnormalities. These results demonstrated the safety profile of our therapeutic intervention with respect to these critical organs.

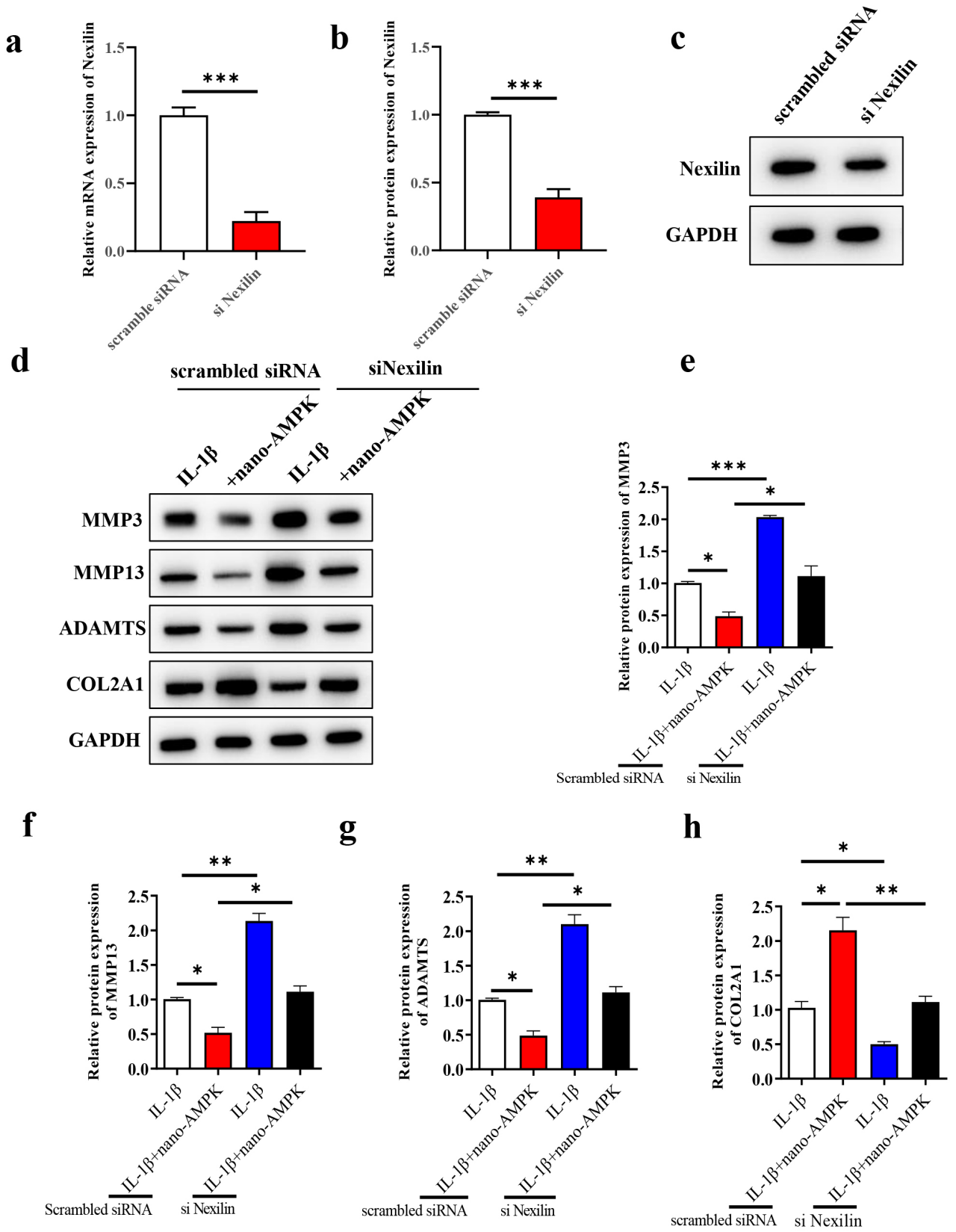

Fig. 5. Inhibited Nexilin reduced matrix degradation markers in IL-1β-stimulated chondrocytes. (**a–c**) mRNA and protein analysis of Nexilin. (**d–h**) Protein analysis of chondrocyte matrix degradation markers. siRNA, small interfering RNA; mRNA, messenger ribonucleic acid. Data are mean ± SD (n = 3), *$p < 0.05$, **$p < 0.01$, and ***$p < 0.001$.

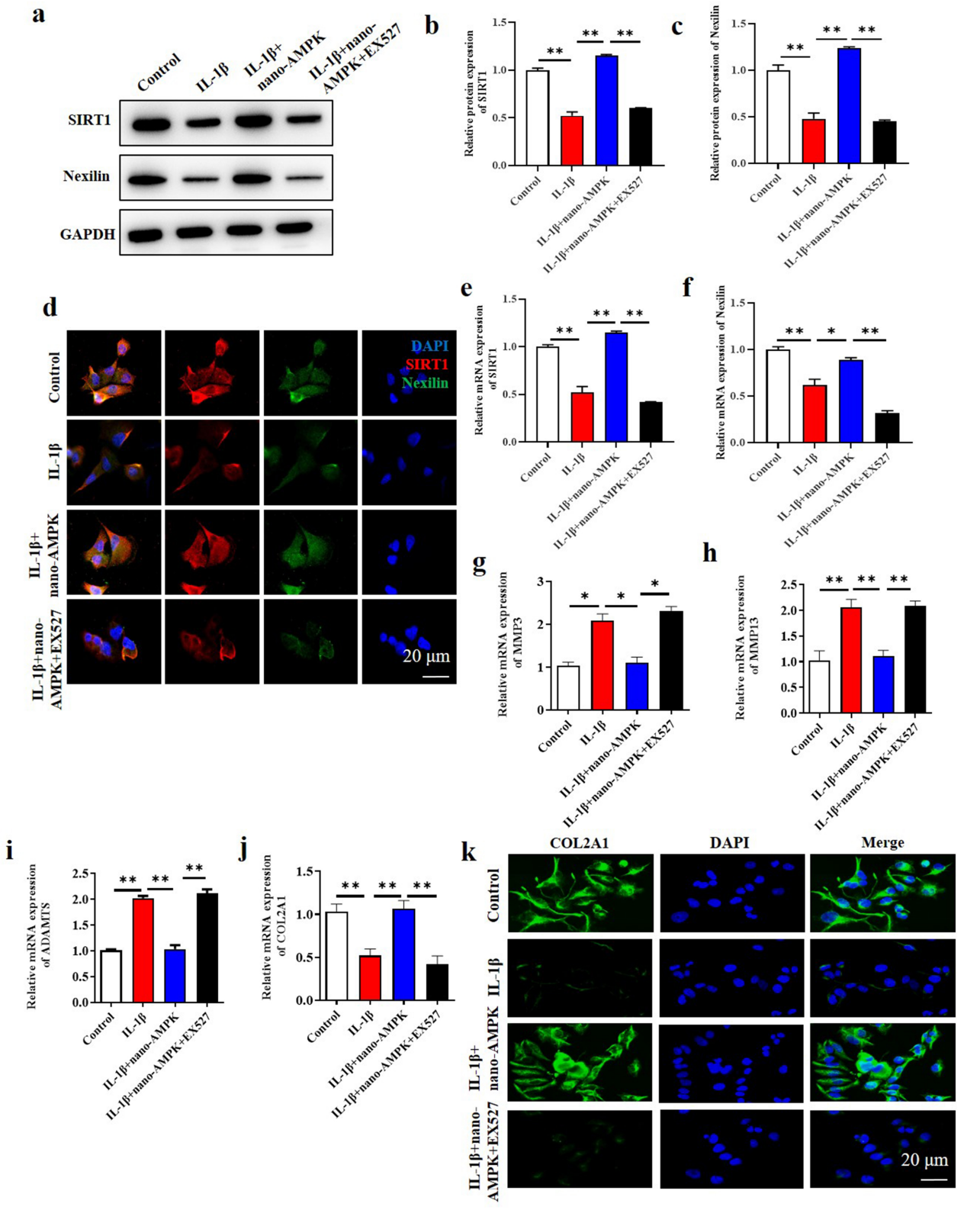

Fig. 6. EX527 reduced SIRT1/Nexilin levels and reversed the inhibitory effects of nano-AMPK on IL-1β-induced chondrocyte matrix degradation markers. (**a–c**) Western blot analysis showing co-expression patterns of SIRT1 and Nexilin under different treatment conditions. (**d**) Double immunofluorescence staining revealed significant co-localization between SIRT1 and Nexilin in chondrocytes. Scale bar: 20 μm. (**e,f**) mRNA expression of SIRT1 and Nexilin. (**g–j**) Expression levels of chondrocyte matrix degradation markers. (**k**) Immunofluorescence (IF) staining to measure COL2A1 intensity in chondrocytes. Scale bar: 20 μm. Data are mean ± SD (n = 3), *$p < 0.05$, **$p < 0.01$.

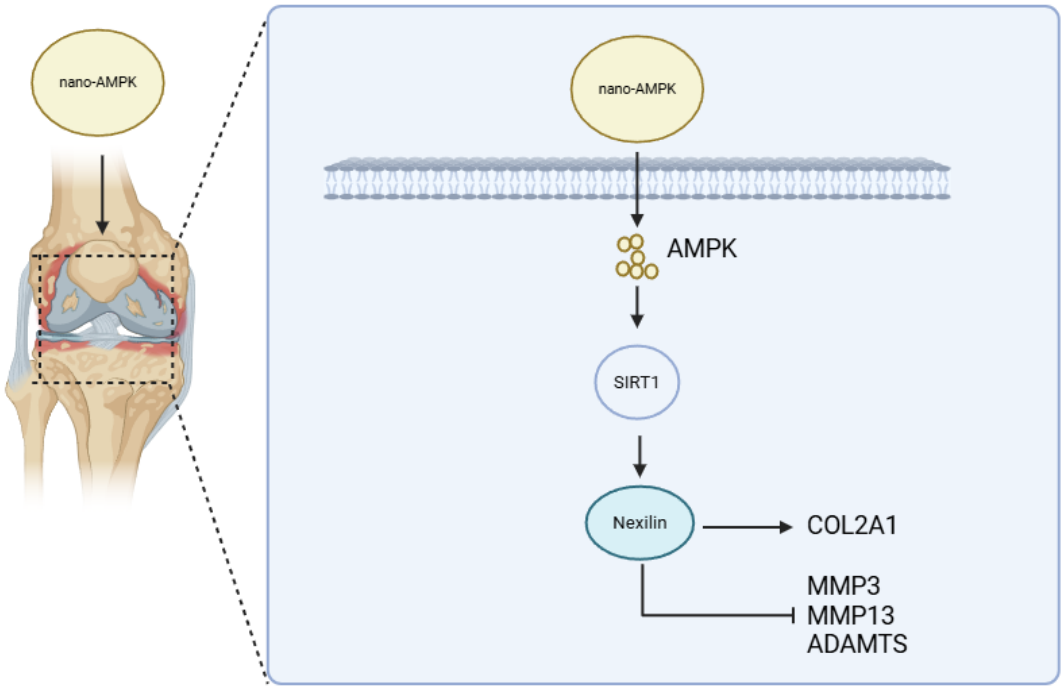

Fig. 7. Action mechanism diagram of nano-AMPK.

Nano-AMPK Co-Culture with IL-1β Boosts Chondrocyte Proliferation and Elevates SIRT1 Expression

To validate the identity and purity of isolated chondrocytes, we performed comprehensive characterization analyses (**Supplementary Fig. S3**). Phase-contrast microscopy revealed that the isolated cells maintained typical chondrocyte morphology through early passages (P0–P2), displaying characteristic polygonal shapes with appropriate size distribution. The chondrocyte phenotype was further confirmed by immunofluorescence staining of key markers, including COL2A1, SOX-9 (a chondrocyte-specific transcription factor), and aggrecan (an essential cartilage matrix protein). These markers showed positive expression, confirming the successful isolation and maintenance of chondrocyte phenotype in our experimental system. Fig. 3**a** illustrates the decrease in chondrocyte proliferation after IL-1β treatment and the increase in chondrocyte proliferation after nano-AMPK treatment ($p < 0.01$). IL-1β reduced AMPK and SIRT1 expression ($p < 0.05$), but nano-AMPK reversed this phenomenon (Fig. 3**b–e**; $p < 0.001$). In addition, the Nexilin protein level in the IL-1β group significantly decreased ($p < 0.01$) but significantly increased after nano-AMPK treatment ($p < 0.01$). We also found that TGF-β1 and Smad2 expression increased in the IL-1β group ($p < 0.01$), but nano-AMPK significantly mitigated this (Fig. 3**f–h**) ($p < 0.01$). The activity of SIRT1 also increased significantly in the IL-1β + nano-AMPK group (Fig. 3**i**) ($p < 0.01$).

Nano-AMPK Reduces Matrix Degradation Markers in IL-1β-Stimulated Chondrocytes

Western blot (Fig. 4**a–h**) showed higher MMP-3, MMP-13, ADAMTS, iNOS, COX-2, and COL2A1 levels in the nano-AMPK group than in the control group ($p < 0.05$).

Nexilin Inhibition Reverses Nano-AMPK's Suppression of IL-1β-Induced Chondrocyte Matrix Degradation Markers

To further investigate the role of Nexilin in nano-AMPK regulation of chondrocyte matrix degradation, messenger ribonucleic acid (mRNA) and Western blot results confirmed that Nexilin expression was silenced using siRNA (Fig. 5**a–c**; $p < 0.001$). In IL-1β-stimulated chondrocytes, MMP-3, MMP-13, ADAMTS, iNOS, and COX-2 levels increased but COL2A1 decreased ($p < 0.05$). Nano-AMPK significantly reduced chondrocyte matrix degradation markers levels and increased COL2A1 ($p < 0.05$). Silencing Nexilin reversed these effects (Fig. 5**d–g**). Additionally, we found that IL-1β significantly reduced COL2A1 expression, and Nexilin knockdown further exacerbated this reduction (Fig. 5**h**; $p < 0.05$).

EX527 Reduced SIRT1/Nexilin Levels and Reversed the Inhibitory Effects of Nano-AMPK on IL-1β-Induced Chondrocyte Matrix Degradation Markers

To further explore the role of SIRT1 in the regulation of chondrocyte matrix degradation by nano-AMPK, we used the SIRT1 inhibitor EX527. Fig. 6**a–c** shows that IL-1β significantly reduced SIRT1 and Nexilin expression

compared with the control group ($p < 0.01$). Nano-AMPK mitigated this reduction ($p < 0.01$), and EX527 reversed the effects of nano-AMPK ($p < 0.01$). Double immunofluorescence staining revealed significant co-localization between SIRT1 and Nexilin in chondrocytes. In control conditions, SIRT1 (red) and Nexilin (green) showed strong co-localization, primarily in the cytoplasm, as evidenced by the yellow overlay signals. IL-1β stimulation markedly decreased SIRT1 and Nexilin expression levels, with reduced co-localization intensity. Notably, nano-AMPK treatment restored the co-localization pattern to levels comparable to the control group, whereas EX527 (SIRT1 inhibitor) treatment significantly attenuated this effect (Fig. 6**d**). These findings provide direct visual evidence for the spatial relationship between SIRT1 and Nexilin, supporting their functional interaction in the context of OA pathogenesis. qRT-PCR results of SIRT1 and Nexilin were consistent with Western blot results (Fig. 6**e,f**). qRT-PCR results showed that in IL-1β-stimulated chondrocytes, MMP-3, MMP-13, and ADAMTS levels increased ($p < 0.05$) but COL2A1 levels decreased ($p < 0.05$). The IL-1β + nano-AMPK + EX527 group showed similar trends ($p < 0.05$). Nano-AMPK reduced MMP-3, MMP-13, and ADAMTS ($p < 0.05$), but EX527 reversed these effects (Fig. 6**g–j**, $p < 0.01$). Fig. 6**k** shows that upregulated COL2A1 was significantly enhanced in the nano-AMPK group, and EX527 reversed this trend ($p < 0.01$). Fig. 7 illustrates a possible mechanism of action of nano-AMPK.

Discussion

A study has shown the potential of nanotechnology in treating OA. This study investigated nano-AMPK's protective effects on cartilage. To determine if nano-AMPK can slow arthritis progression, we administered intra-articular injections in an ACLT-induced OA model. The nano-AMPK group had increased AMPK levels. Compared with the model group, the nano-AMPK group had significantly lower levels of iNOS, COX-2, PGE2, and TNF-α. iNOS, which produces nitric oxide (NO), is elevated in inflammatory conditions and induces the release of MMP-3 and MMP-13, key factors in OA pathogenesis [19–21]. Additionally, TNF-α promotes NO production and is linked to apoptosis and pain in patients with OA [22]. Previous studies indicated that AMPK may reduce NO, IL-1β, and TNF-α through antioxidant and anti-inflammatory effects, thereby decreasing cartilage degradation [23–25]. COX-2, related to pain and inflammation, is abnormally elevated by IL-1β and TNF-α [25–27]. Currently, nonsteroidal antiinflammatory drugs (NSAIDs) are clinically used to inhibit COX-2, offering anti-inflammatory and analgesic effects. Thus, nano-AMPK may also provide anti-inflammatory, analgesic, and cartilage-protective benefits in an OA rat model.

Masson staining showed that the cartilage structure and ECM in the nano-AMPK group remained relatively intact compared with the model group. Nano-AMPK protected articular cartilage in ACLT-induced OA rats. Research suggested that AMPK mitigates OA progression by regulating cartilage matrix homeostasis [28]. Nano-AMPK increased the expression of cartilage markers like COL2A1 and aggrecan while reducing catabolic markers and apoptotic indicators. Additionally, AMPK promotes TGF-β1 expression in chondrocytes, facilitating ECM synthesis [29,30]. *In vivo* experiments demonstrated that nano-AMPK alleviates OA progression.

Our studies showed that nano-AMPK reduced MMP-3, MMP-13, and ADAMTS but increased COL2A1 and aggrecan. ADAMTS and MMP-3 are key ECM-degrading enzymes and markers of joint degeneration [31]. AMPK increased SOX-9 and COL2A1 but decreased matrix degradation proteins [32]. Additionally, nano-AMPK significantly reduced iNOS and COX-2 expression in IL-1β-induced chondrocytes. Excessive iNOS produces NO, which inhibits proteoglycan and collagen synthesis, activates metalloproteinases, induces apoptosis, and regulates inflammation. A Study suggested that nano-AMPK may inhibit cartilage matrix degradation proteins by reducing oxidative stress, but specific mechanisms need further investigation [33].

To elucidate nano-AMPK's mechanisms in OA, we conducted *in vitro* experiments. CCK-8 assay results indicated that nano-AMPK co-cultured with IL-1β showed no cytotoxic effects on chondrocytes. IL-1β induces inflammation through multiple pathways and promotes MMP and pro-inflammatory mediator secretion, accelerating cartilage destruction [34]. Therefore, IL-1β was used to mimic the OA environment in our experiments. Nexilin, an actin-associated protein involved in cytoskeletal remodeling and stabilization, plays a role in chondrocyte mechanical stress response and matrix metabolism. We reversed nano-AMPK's therapeutic effects by inhibiting Nexilin expression. Furthermore, SIRT1 protects chondrocytes by reducing oxidative stress and inflammation, combating OA [35,36]. Conversely, in IL-1β-stimulated chondrocytes, AMPK suppresses SIRT1 expression and activity, lowering MMP-3 and MMP-13 levels [37]. AMPK treatment shows antitumor activity in human osteosarcoma cells by inhibiting the SIRT1 pathway, indicating that it targets this pathway. To confirm the relationship between nano-AMPK and SIRT1 in IL-1β-induced chondrocytes, we used the SIRT1 inhibitor EX527. Our findings showed that IL-1β and EX527 reduced SIRT1 expression. Nano-AMPK restored SIRT1 levels reduced by IL-1β but not by EX527, confirming nano-AMPK's activation of SIRT1.

Nano-AMPK significantly boosted COL2A1 expression and mRNA levels in IL-1β-induced chondrocytes. COL2A1, secreted by chondrocytes into the ECM, serves a protective role. The capacity of nano-AMPK to restore cartilage may be related to the rise in COL2A1. Adhesion, migration, differentiation, and ECM formation all de-

pend on high TGF-β1 levels in cartilage [38,39]. Nano-AMPK activates the TGF-β1/Smad2 pathway, but EX527 did not negate this effect, indicating that SIRT1 was not involved. In hepatocytes and nephropathic epithelial cells, SIRT1 upregulation inhibits the TGF-β1/Smads pathway [40]. The connection between SIRT1 and the chondrocyte TGF-β1/Smad2 pathway is not documented in any research. Nano-AMPK's enhancement of COL2A1 may relate to TGF-β1 activation. However, EX527 inhibited COL2A1, suggesting that the benefits of TGF-β1/Smad2 activation were less than the negative effects of SIRT1 inhibition. The robust upregulation of COL2A1 by nano-AMPK treatment represents a significant therapeutic advantage in OA management. COL2A1 restoration is particularly important because it not only provides structural support but also creates a favorable microenvironment for chondrocyte survival and function. Our findings showed that increased COL2A1 levels were correlated with enhanced mechanical properties of the cartilage matrix, as evidenced by improved tissue architecture in histological analyses. The maintenance of COL2A1 levels through nano-AMPK treatment may help break the destructive cycle of OA progression by stabilizing the ECM structure and reducing mechanical stress-induced damage. This mechanism suggested that early intervention with nano-AMPK may slow or halt OA progression by preserving cartilage matrix integrity through sustained COL2A1 expression. Furthermore, the parallel improvement in inflammatory markers and matrix-degrading enzymes indicated that COL2A1 upregulation is part of a broad protective mechanism that could have lasting benefits for cartilage health.

Our study advances the field of nano-based OA therapeutics in several key aspects. First, while previous nanocarrier systems primarily focused on drug delivery, our approach demonstrates the feasibility of delivering active proteins while maintaining their biological function. Second, unlike conventional AMPK activators that work systemically, our nano-encapsulation strategy enables more targeted delivery to the affected cartilage. Third, our work revealed a previously unknown SIRT1-Nexilin pathway in OA pathogenesis, providing new therapeutic targets for future nanomedicine development. These findings build upon recent studies showing the importance of targeted delivery systems in OA treatment, while addressing the crucial challenge of protein therapeutic delivery. Although our study provides strong evidence for nano-AMPK's protective effects through the SIRT1-Nexilin pathway, we acknowledge several limitations. First, OA is a complex disease involving multiple signaling cascades, including nuclear factor kappa-B (NF-κB) and mitogen-activated protein kinase (MAPK) pathways, which were not extensively investigated in this study. The potential cross-talk between SIRT1-Nexilin and these pathways warrants further investigation. Second, the comparative efficacy of nano-AMPK versus standard treatments remains to be established. Future studies should explore potential synergistic effects between nano-AMPK and conventional therapeutics such as NSAIDs or corticosteroids. Additionally, investigating the interaction between SIRT1-Nexilin and other inflammatory pathways could provide a comprehensive understanding of nano-AMPK's therapeutic mechanism. These investigations would further strengthen the translational potential of nano-AMPK in OA treatment.

Our studies showed that EX527 increased MMP-3, MMP-13, ADAMTS, iNOS, and COX-2 levels but decreased COL2A1. Nano-AMPK did not alter these results, indicating that SIRT1 inhibition raised the risk of matrix degradation. In IL-1β-stimulated chondrocytes, nano-AMPK counteracted reduced SIRT1 expression and decreased matrix degradation proteins, thereby protecting chondrocytes.

Conclusions

Nano-AMPK demonstrated significant protective effects against cartilage degradation in experimental OA. Our findings revealed that nano-AMPK functions through the SIRT1-Nexilin pathway to reduce matrix degradation and inflammation in cartilage tissue. This result was confirmed through SIRT1 inhibition by EX527 and Nexilin knockdown experiments, which reversed nano-AMPK's protective effects. The dual validation in ACLT rat models and IL-1β-induced chondrocytes provides strong evidence for nano-AMPK's therapeutic potential in OA treatment. These findings offer new insights into the molecular mechanisms of nano-encapsulated active protein AMPK and provide a theoretical foundation for developing novel OA therapeutic strategies.

List of Abbreviations

ACLT, anterior cruciate ligament transection; ADAMTS, a disintegrin and metalloproteinase with thrombospondin motifs; AMPK, adenosine monophosphate-activated protein kinase; CCK-8, Cell Counting Kit-8; COL2A1, collagen type II alpha 1 chain; COX-2, cyclooxygenase-2; DL, drug loading; DMEM, Dulbecco's modified Eagle medium; DMSO, dimethyl sulfoxide; ECM, extracellular matrix; EE, encapsulation efficiency; ELISA, enzyme-linked immunosorbent assay; FBS, fetal bovine serum; GAPDH, glyceraldehyde 3-phosphate dehydrogenase; H&E, hematoxylin and eosin; IHC, immunohistochemical; IL-1β, interleukin-1 beta; iNOS, inducible nitric oxide synthase; MMP, matrix metalloproteinase; OA, osteoarthritis; qRT-PCR, quantitative real-time polymerase chain reaction; SD, standard deviation; siRNA, small interfering RNA; SIRT1, sirtuin 1; TEM, transmission electron microscopy; TGF-β, transforming growth factor beta; TNF-α, tumor necrosis factor alpha; DLS, dynamic light scattering; IF, Immunofluorescence; ns, not significant; NAD+, nicotinamide adenine dinucleotide; PBS, phosphate buffer saline; STR, short

tandem repeat; DAPI, 4′,6-diamidino-2′-phenylindole; SDS-PAGE, sodium dodecyl sulfate polyacrylamide gel electrophoresis; PVDF, polyvinylidene fluoride; ANOVA, analysis of variance; mRNA, messenger ribonucleic acid.

Availability of Data and Materials

The datasets used and/or analysed during the current study were available from the corresponding author on reasonable request.

Author Contributions

XY and LLF designed the study. QQW and XY collected and analyzed the data. BRQ and LQW participated in drafting the manuscript. All authors conducted the study and contributed to critical revision of the manuscript for important intellectual content. All authors gave final approval of the version to be published. All authors participated fully in the work, took public responsibility for appropriate portions of the content, and agreed to be accountable for all aspects of the work in ensuring that questions related to the accuracy or completeness of any part of the work were appropriately investigated and resolved.

Ethics Approval and Consent to Participate

The research protocol was approved by the Ethics Committee of Harbin Zhongke Saines Biotechnology Co. (Ethic Approval Number: HRBSCIEC20230301), and all animal procedures were performed in accordance with the Guidelines for the Care and Use of Laboratory Animals of Harbin Zhongke Saines Biotechnology Co.

Acknowledgments

Not applicable.

Funding

This research was funded by Supported by Hainan Provincial Natural Science Foundation of China (821MS163), and Joint Program on Health Science & Technology Innovation of Hainan Province (WSJK2024MS208).

Conflict of Interest

The authors declare no conflict of interest.

Supplementary Material

Supplementary material associated with this article can be found, in the online version, at https://doi.org/10.22203/eCM.v050a07.

References

[1] Felson DT, Lawrence RC, Hochberg MC, McAlindon T, Dieppe PA, Minor MA, *et al*. Osteoarthritis: new insights. Part 2: treatment approaches. Annals of Internal Medicine. 2000; 133: 726–737. https://doi.org/10.7326/0003-4819-133-9-200011070-00015.

[2] Gildea E, Scales-Theobald E, Thompson J, Cook A, Forde K, Skingley G, *et al*. Development and validation of a quality of life and treatment satisfaction measure in canine osteoarthritis. Frontiers in Veterinary Science. 2024; 11: 1377019. https://doi.org/10.3389/fvets.2024.1377019.

[3] Wang J, Li J, Song D, Ni J, Ding M, Huang J, *et al*. AMPK: implications in osteoarthritis and therapeutic targets. American Journal of Translational Research. 2020; 12: 7670–7681.

[4] Li J, Zhang B, Liu WX, Lu K, Pan H, Wang T, *et al*. Metformin limits osteoarthritis development and progression through activation of AMPK signalling. Annals of the Rheumatic Diseases. 2020; 79: 635–645. https://doi.org/10.1136/annrheumdis-2019-216713.

[5] Lim HD, Kim YS, Ko SH, Yoon IJ, Cho SG, Chun YH, *et al*. Cytoprotective and anti-inflammatory effects of melatonin in hydrogen peroxide-stimulated CHON-001 human chondrocyte cell line and rabbit model of osteoarthritis via the SIRT1 pathway. Journal of Pineal Research. 2012; 53: 225–237. https://doi.org/10.1111/j.1600-079X.2012.00991.x.

[6] Xing H, Liang C, Wang C, Xu X, Hu Y, Qiu B. Metformin mitigates cholesterol accumulation via the AMPK/SIRT1 pathway to protect osteoarthritis chondrocytes. Biochemical and Biophysical Research Communications. 2022; 632: 113–121. https://doi.org/10.1016/j.bbrc.2022.09.074.

[7] Zhao Z, Liu Y, Lu Y, Hou M, Shen X, Yang H, *et al*. Gingko bilobainspired lactone prevents osteoarthritis by activating the AMPK-SIRT1 signaling pathway. Arthritis Research & Therapy. 2022; 24: 197. https://doi.org/10.1186/s13075-022-02890-y.

[8] Liu C, Spinozzi S, Chen JY, Fang X, Feng W, Perkins G, *et al*. Nexilin Is a New Component of Junctional Membrane Complexes Required for Cardiac T-Tubule Formation. Circulation. 2019; 140: 55–66. https://doi.org/10.1161/circulationaha.119.039751.

[9] Spinozzi S, Liu C, Chen Z, Feng W, Zhang L, Ouyang K, *et al*. Nexilin Is Necessary for Maintaining the Transverse-Axial Tubular System in Adult Cardiomyocytes. Circulation. Heart Failure. 2020; 13: e006935. https://doi.org/10.1161/circheartfailure.120.006935.

[10] Yu M, Wu J, Shi J, Farokhzad OC. Nanotechnology for protein delivery: Overview and perspectives. Journal of Controlled Release: Official Journal of the Controlled Release Society. 2016; 240: 24–37. https://doi.org/10.1016/j.jconrel.2015.10.012.

[11] Wong HL, Wu XY, Bendayan R. Nanotechnological advances for the delivery of CNS therapeutics. Advanced Drug Delivery Reviews. 2012; 64: 686–700. https://doi.org/10.1016/j.addr.2011.10.007.

[12] Yi D, Yu H, Lu K, Ruan C, Ding C, Tong L, *et al*. AMPK signaling in energy control, cartilage biology, and osteoarthritis. Frontiers in Cell and Developmental Biology. 2021; 9: 696602.

[13] Chen Y, Liu Y, Jiang K, Wen Z, Cao X, Wu S. Linear ubiquitination of LKB1 activates AMPK pathway to inhibit NLRP3 inflammasome response and reduce chondrocyte pyroptosis in osteoarthritis. Journal of Orthopaedic Translation. 2023; 39: 1–11

[14] Markel JE, Lacinski RA, Lindsey BA. Nanocapsule Delivery of IL-12. Advances in Experimental Medicine and Biology. 2020; 1257: 155–168. https://doi.org/10.1007/978-3-030-43032-0_13.

[15] Hamdalla HM, Ahmed RR, Galaly SR, Naguib IA, Alghamdi BS, Ahmed OM, *et al*. Ameliorative Effect of Curcumin Nanoparticles against Monosodium Iodoacetate-Induced Knee Osteoarthritis in Rats. Mediators of Inflammation. 2022; 2022: 8353472. https://doi.org/10.1155/2022/8353472.

[16] Zhou S, Shi J, Wen H, Xie W, Han X, Li H. A chondroprotective effect of moracin on IL-1β-induced primary rat chondrocytes and an osteoarthritis rat model through Nrf2/HO-1 and NF-κB axes. Food & Function. 2020; 11: 7935–7945. https://doi.org/10.1039/d0fo01496f.

[17] Zhang Y, Jiang H, Du J, Ming J, Li Y, Ma Y, *et al*. Nanoparticle-activated SIRT3/SOD2 axis involves amelioration of chondrocyte senescence to delay osteoarthritis progression. Chemical Engineering Journal. 2024; 497: 154799. https://doi.org/https://doi.org/10.1016/j.cej.2024.154799.

[18] Liang C, Xing H, Wang C, Xu X, Hao Y, Qiu B. Resveratrol protection against IL-1β-induced chondrocyte damage via the SIRT1/FOXO1 signaling pathway. Journal of Orthopaedic Surgery and Research. 2022; 17: 406. https://doi.org/10.1186/s13018-022-03306-y.

[19] Maldonado M, Nam J. The role of changes in extracellular matrix of cartilage in the presence of inflammation on the pathology of osteoarthritis. BioMed Research International. 2013; 2013: 284873. https://doi.org/10.1155/2013/284873.

[20] Cipolletta C, Jouzeau JY, Gegout-Pottie P, Presle N, Bordji K, Netter P, *et al*. Modulation of IL-1-induced cartilage injury by NO synthase inhibitors: a comparative study with rat chondrocytes and cartilage entities. British Journal of Pharmacology. 1998; 124: 1719–1727. https://doi.org/10.1038/sj.bjp.0702005.

[21] Clynes MA, Jameson KA, Edwards MH, Cooper C, Dennison EM. Impact of osteoarthritis on activities of daily living: does joint site matter? Aging Clinical and Experimental Research. 2019; 31: 1049–1056. https://doi.org/10.1007/s40520-019-01163-0.

[22] Wang Y, Che M, Xin J, Zheng Z, Li J, Zhang S. The role of IL-1β and TNF-α in intervertebral disc degeneration. Biomedicine & Pharmacotherapy = Biomédecine & Pharmacothérapie. 2020; 131: 110660. https://doi.org/10.1016/j.biopha.2020.110660.

[23] Wang Y, Tian M, Tan J, Pei X, Lu C, Xin Y, *et al*. Irisin ameliorates neuroinflammation and neuronal apoptosis through integrin αVβ5/AMPK signaling pathway after intracerebral hemorrhage in mice. Journal of Neuroinflammation. 2022; 19: 82. https://doi.org/10.1186/s12974-022-02438-6.

[24] Chen S, Peng J, Sherchan P, Ma Y, Xiang S, Yan F, *et al.* TREM2 activation attenuates neuroinflammation and neuronal apoptosis via PI3K/Akt pathway after intracerebral hemorrhage in mice. Journal of Neuroinflammation. 2020; 17: 168. https://doi.org/10.1186/s12974-020-01853-x.

[25] Rodríguez MI, Escames G, López LC, López A, García JA, Ortiz F, *et al*. Chronic melatonin treatment reduces the age-dependent inflammatory process in senescence-accelerated mice. Journal of Pineal Research. 2007; 42: 272–279. https://doi.org/10.1111/j.1600-079X.2006.00416.x.

[26] Carrillo-Vico A, Lardone PJ, Naji L, Fernández-Santos JM, Martín-Lacave I, Guerrero JM, *et al*. Beneficial pleiotropic actions of melatonin in an experimental model of septic shock in mice: regulation of pro-/anti-inflammatory cytokine network, protection against oxidative damage and anti-apoptotic effects. Journal of Pineal Research. 2005; 39: 400–408. https://doi.org/10.1111/j.1600-079X.2005.00265.x.

[27] Muchamuel T, Menon S, Pisacane P, Howard MC, Cockayne DA. IL-13 protects mice from lipopolysaccharide-induced lethal endotoxemia: correlation with down-modulation of TNF-alpha, IFN-gamma, and IL-12 production. The Journal of Immunology: Official Journal of the American Association of Immunologists. 1997; 158: 2898–2903.

[28] Zhang S, Teo KYW, Chuah SJ, Lai RC, Lim SK, Toh WS. MSC exosomes alleviate temporomandibular joint osteoarthritis by attenuating inflammation and restoring matrix homeostasis. Biomaterials. 2019; 200: 35–47. https://doi.org/10.1016/j.biomaterials.2019.02.006.

[29] Zou J, Li C, Jiang S, Luo L, Yan X, Huang D, *et al*. AMPK inhibits Smad3-mediated autoinduction of TGF-β1 in gastric cancer cells. Journal of Cellular and Molecular Medicine. 2021; 25: 2806–2815. https://doi.org/10.1111/jcmm.16308.

[30] Li NS, Zou JR, Lin H, Ke R, He XL, Xiao L, *et al*. LKB1/AMPK inhibits TGF-β1 production and the TGF-β signaling pathway in breast cancer cells. Tumour Biology: the Journal of the International Society for Oncodevelopmental Biology and Medicine. 2016; 37: 8249–8258. https://doi.org/10.1007/s13277-015-4639-9.

[31] Lim H, Kim DK, Kim TH, Kang KR, Seo JY, Cho SS, *et al*. Acteoside Counteracts Interleukin-1β-Induced Catabolic Processes through the Modulation of Mitogen-Activated Protein Kinases and the NFκB Cellular Signaling Pathway. Oxidative Medicine and Cellular Longevity. 2021; 2021: 8684725. https://doi.org/10.1155/2021/8684725.

[32] Loeser RF, Beavers DP, Bay-Jensen AC, Karsdal MA, Nicklas BJ, Guermazi A, *et al*. Effects of dietary weight loss with and without exercise on interstitial matrix turnover and tissue inflammation biomarkers in adults with knee osteoarthritis: the Intensive Diet and Exercise for Arthritis trial (IDEA). Osteoarthritis and Cartilage/OARS, Osteoarthritis Research Society. 2017; 25: 1822–1828. https://doi.org/10.1016/j.joca.2017.07.015.

[33] Sun K, Jing X, Guo J, Yao X, Guo F. Mitophagy in degenerative joint diseases. Autophagy. 2021; 17: 2082–2092. https://doi.org/10.1080/15548627.2020.1822097.

[34] Fu H, Zhou D, Zhu H, Liao J, Lin L, Hong X, *et al.* Matrix metalloproteinase-7 protects against acute kidney injury by priming renal tubules for survival and regeneration. Kidney International. 2019; 95: 1167–1180. https://doi.org/10.1016/j.kint.2018.11.043.

[35] Guo Y, Chao L, Chao J. Kallistatin attenuates endothelial senescence by modulating Let-7g-mediated miR-34a-SIRT1-eNOS pathway. Journal of Cellular and Molecular Medicine. 2018; 22: 4387–4398. https://doi.org/10.1111/jcmm.13734.

[36] Oka SI, Byun J, Huang CY, Imai N, Ralda G, Zhai P, *et al*. Nampt Potentiates Antioxidant Defense in Diabetic Cardiomyopathy. Circulation Research. 2021; 129: 114–130. https://doi.org/10.1161/circresaha.120.317943.

[37] Terauchi K, Kobayashi H, Yatabe K, Yui N, Fujiya H, Niki H, *et al*. The NAD-Dependent Deacetylase Sirtuin-1 Regulates the Expression of Osteogenic Transcriptional Activator Runt-Related Transcription Factor 2 (Runx2) and Production of Matrix Metalloproteinase (MMP)-13 in Chondrocytes in Osteoarthritis. International Journal of Molecular Sciences. 2016; 17: 1019. https://doi.org/10.3390/ijms17071019.

[38] Lee DY, Choi SI, Han SH, Lee YJ, Choi JG, Lee YS, *et al*. Potential of Pseudoshikonin I Isolated from Lithospermi Radix as Inhibitors of MMPs in IL-1β-Induced SW1353 Cells. International Journal of Molecular Sciences. 2016; 17: 1350. https://doi.org/10.3390/ijms17081350.

[39] Lee HJ, Lee SM, Moon YG, Jung YS, Lee JH, Venkatarame Gowda Saralamma V, *et al*. Membrane-Free Stem Cell Components Inhibit Interleukin-1α-Stimulated Inflammation and Cartilage Degradation *in vitro* and *in vivo*: A Rat Model of Osteoarthritis. International Journal of Molecular Sciences. 2019; 20: 4869. https://doi.org/10.3390/ijms20194869.

[40] Yang YZ, Zhao XJ, Xu HJ, Wang SC, Pan Y, Wang SJ, *et al*. Magnesium isoglycyrrhizinate ameliorates high fructose-induced liver fibrosis in rat by increasing miR-375-3p to suppress JAK2/STAT3 pathway and TGF-β1/Smad signaling. Acta Pharmacologica Sinica. 2019; 40: 879–894. https://doi.org/10.1038/s41401-018-0194-4.

Editor's note: The Scientific Editor responsible for this paper was Juerg Gasser.

Received: 23rd October 2024; **Accepted**: 23rd December 2024; **Published**: 24th April 2025